www.sciencemag.org/content/342/6164/1351/suppl/DC1

Supplementary Materials for

Effect of Collective Molecular Reorientations on Brownian Motion of Colloids in Nematic Liquid Crystal

T. Turiv, I. Lazo, A. Brodin, B. I. Lev, V. Reiffenrath, V. G. Nazarenko, O. D. Lavrentovich*

*Corresponding author. E-mail: olavrent@kent.edu

Published 13 December 2013, *Science* **342**, 1351 (2013)
DOI: 10.1126/science.1240591

This PDF file includes:

Materials and methods

Materials

We used silica spheres of diameter d = 1.6, 3, 5, 6.5, 8, and 10 μm (Bangs Laboratories), with two types of surface alignment: perpendicular, Fig. 1A, and tangential to the particle's surface, Fig. 1B. In the first case, the spheres were functionalized with octadecyl-dimethyl(3-trimethoxysilylpropyl) ammonium chloride (DMOAP) (*32*). In the second case, the particles were left untreated. The overall uniform orientation of the nematic was set by two glass plates covered with rubbed polyimide PI-2555 (Nissan Chemicals) that produces a unidirectional planar alignment. The locally distorted director around the spheres must smoothly transform into the uniform field far away from it. The resulting equilibrium director is either of a dipolar type (with a point defect-hyperbolic hedgehog accompanying the sphere) for normal anchoring, Fig. 1A, or of a quadrupolar type with two surface defects-boojums at the poles, in the tangential anchoring case, Fig. 1B (*30*). The director distortions around the particle (*22*) cause repulsion from the bounding substrates, so that the colloid levitates in the bulk at some height determined by the balance of gravity and elastic forces (*23*), Fig. S1.

To minimize the image drifting in highly birefringent medium we use the nematic IS-8200 (*24*), Fig. S2 and Table S1, with ultra-low birefringence $\Delta n = 0.0015$ (at $\lambda = 520$ nm) that is two orders of magnitude smaller than birefringence of a standard nematic pentylcyanobiphenyl (5CB) with $\Delta n = 0.17$. For $R \sim 5$ μm, the image drift in IS-8200 is less than ~ 10 nm. We also studied 5CB and a lyotropic nematic, formed by water solutions of disodium chromoglycate (DSCG) with a relatively low negative birefringence $\Delta n = -0.015$ (at $\lambda = 520$ nm).

Methods

Particle Tracking

We used high-speed video camera MotionBlitz EoSens mini1 (Microtron GmbH) mounted on an inverted microscope Nikon ECLIPSE TE2000-U with a 100× 1.3 N.A. immersion objective to trace the particle trajectories. To control the temperature, we used the heating stage Linkam LTS120 (accuracy 0.1°C). Digital images of isolated colloidal particles, captured at a maximum frame rate of 2400 fps (time resolution 0.4 ms), were analyzed to find the coordinates (x, y) of the particle's center using the intensity-weighted algorithms (*33*).

Sequences of images were tracked continuously for more than 100 s. As discussed in the main text, tracking of the particle's position in a LC is complicated by birefringence of the material. To establish the limit of accuracy in measurements of particle's positions that depends on birefringence, we used particles immobilized (by a Norland adhesive) at the bottom plate of the cell filled with the LC. First, we determined the coordinates of immobilized particles in an empty cell, as $x = \frac{\sum_i I_i x_i}{\sum_i I_i}$ and $y = \frac{\sum_i I_i y_i}{\sum_i I_i}$, where x_i and y_i are the coordinates of the *i*-th pixel, I_i is its intensity, Fig. S3. Within each frame with 8-bit gray scale (0-255 arbitrary units of intensity), only the pixels with intensity higher than a certain threshold value $I_{i,threshold}$ were taken into account; $I_{i,threshold}$ was determined from the condition that the mean square displacement of the immobilized particle is minimum, Figure S3E.

The experiments with the empty cells were followed by experiments with cells filled with five different fluids: three types of a nematic LC and two isotropic fluids (water and glycerol). In all cases, we determined the MSD of particles immobilized at the bottom plate, to maximize the effect of the medium on the measured MSD. The probing light beam travelled through the entire thickness of the cell. The apparent mean square displacement of the immobilized particles versus time lag is shown in Fig. S4. The apparent displacements represent a cumulative effect of errors in measuring the particle's position caused by the optical system of the microscope, vibrations and birefringence. It grows with birefringence of the material, being the largest for the nematic pentylcyanobiphenyl (5CB) with the highest birefringence (~0.2). In all cases, the apparent MSD in the time range of interest was about 10^{-16} m^2 or less; these values are about 100 times smaller than the MSD of free spheres experiencing anomalous diffusion described in the main text.

Because of the long range elastic interaction between particles in a nematic, we used only very low concentrations of the colloidal particles, so that the distance between them is much larger (by a factor of 50 at least) than their diameter. The trajectories were measured for individual particles in separate samples. As an example, we show data for cells of the same thickness 50 μm containing similar 5 μm spheres with homeotropic alignment, Fig. S6. The overall behavior of trajectories for different spheres is the same, with some variations of the characteristic times; we attribute these differences to variations of anchoring conditions on the particles surface.

Probability distribution

The difference in diffusion regimes is also examined by measuring the probability distribution of particle displacements. We calculate the probability distribution function $G(\Delta x,\tau)=\frac{1}{N}\sum_{i=1}^{N}\delta\left(\Delta x-\left|x_i(0)-x_i(\tau)\right|\right)$ for displacements parallel to $\hat{\mathbf{n}}_0$, Fig. 4, and a similar function $G(\Delta y,\tau)$ for the perpendicular component (*34*), Fig. S16. Here N is the total number of particle's displacements extracted from the traced trajectory with a time step τ; δ is the Dirac delta function. We determined $G(\Delta x,\tau)$ and $G(\Delta y,\tau)$ for $d =$ $5\ \mu\text{m}$ spheres with normal surface anchoring. The data for a fixed τ are then compared to the Gaussian probability distribution functions, such as $G_G(\Delta x)=\frac{A}{\sigma\sqrt{2\pi}}\exp\left[-\frac{(\Delta x)^2}{2\sigma^2}\right]$, Fig. 4, where σ is the standard deviation of the distribution and A is the normalization constant (and a similar function $G_G(\Delta y)$). The fitting was performed for three different time lags that correspond to the different diffusion regimes suggested by MSD and $C_v(\tau)$ measurements, Fig. 2A-2C.

Connection of MSD and velocity autocorrelation function

The MSD along, say, the *x*-axis is expressed through the velocity autocorrelation function as follows (*25*, *26*):

$$\left\langle\Delta x^2(t)\right\rangle=2\int_0^t dt'\int_0^{t'}C_{V_x}(t'')dt''.$$

Conversely, $C_{V_x}(t)=\frac{1}{2}\frac{d^2\left\langle\Delta x^2(t)\right\rangle}{dt^2}$. Thus, normal diffusion with $\left\langle\Delta x^2(t)\right\rangle\propto t$ would lead to $C_{\mathrm{V}}(t)=0$. If $C_{\mathrm{V}}(t)$ is non-zero, its sign distinguishes subdiffusion ($C_{\mathrm{V}}(t)<0$, the MSD grows slower than t) from superdiffusion ($C_{\mathrm{V}}(t)>0$, the MSD grows faster than t).

SOM Text

1. Director Relaxation Times of IS-8200

To evaluate the relaxation time of director in IS-8200, we used the electric field-induced Frederiks transition (*29*). Since the dielectric anisotropy of IS-8200 is negative, the simplest approach is to explore the director reorientation in the geometry of bend Frederiks effect (*29*). In the field-free state, the director is aligned perpendicularly to the two glass plates. We used SE-1211 polyimide (Nissan Chemical Industries, Ltd.) for this homeotropic alignment; the polymer layers were rubbed in order to pre-select the direction of director tilt when the electric field is applied to the conductive indium tin oxide (ITO) electrodes deposited at the glass plates beneath the polymer layers. We used cells with gaps of thickness 10, 20, 30, 50, and 75 μm.

The cell is kept in the heating stage HS-1 (Instec Inc.) at 50°C and observed between two crossed polarizers aligned at 45 degrees to the rubbing direction. As the voltage exceeds some threshold V_{th}, the director deviates from the vertical orientation and light transmission through the cell increases, Fig. S7. We find V_{th} = 4.7 V for 20 μm cell.

By raising the AC voltage slightly above V_{th} and switching it off, we monitor the relaxation of the optical signal and fit it with the exponential function to determine the relaxation time of bend deformation, Fig. S8. The thickness dependence of relaxation time is shown in Fig. S9; as expected, it follows a quadratic dependence. The ratio $\eta_{eff} / K = 5.8 \times 10^{10}$ s/m^2 is estimated from (*29*):

$$\frac{\eta_{eff}}{K} = \frac{\tau_{\text{relax}} \pi^2}{h^2}.$$

We performed a similar experiment for twist Frederiks transition in a planar cell; planar alignment was achieved by oblique evaporation of SiO_x. The electric field was applied in the plane of the cell. The dynamics of transmitted light intensity is shown in Fig. S10. The deduced effective value in this case is $\eta_{eff} / K = 16 \times 10^{10}$ s/m^2. The typical order-of-magnitude estimate is thus $\eta_{eff} / K \approx 10^{11}$ s/m^2.

2. Diffusion of the particles in 5CB

In the classic nematic 5CB, the MSD dependencies suggest subdiffusion with $\alpha_{\parallel} = 0.38$ and $\alpha_{\perp} = 0.36$, but only when the time lags are shorter than $\tau_{sub}^{\parallel}$ = 8.4 ms and $\tau_{sub}^{\perp}$ = 6.6 ms, Fig. S11. The data are presented for 5 μm particles with normal anchoring at

24°C. At longer times, the diffusion is normal and anisotropic with $D_{\|} = 2.7\times10^{-15}$ m^2/s^{-1} and $D_{\perp} = 1.3\times10^{-15}$ m^2/s^{-1}; the effective viscosities are $\eta_{\|} = 63.5$ mPa s and $\eta_{\perp} = 90.0$ mPa s. These values fall within the range of the Mieşowicz viscosities known for 5CB (42, 22, and 118 mPa s (*35*) and are close to the values $\eta_{\|} = 52.5$ mPa s and $\eta_{\perp} = 86.4$ mPa s, obtained in Ref. (*36*). In the isotropic (40°C) phase, the diffusion is normal and isotropic, with $D = 2.9\times10^{-15}$ m^2/s^{-1}.

3. Diffusion of the particles in lyotropic chromonic liquid crystal DSCG

The experiments on Brownian motion were repeated for the lyotropic chromonic LC disodium chromoglycate (DSCG) (*37*) with $\Delta n = 0.015$ at λ=520 nm (*38*). The nematic phase in the water solution with 13 wt % concentration of DSCG exists at room temperature; it melts into an isotropic phase at 29°C. The elastic constants at the studied temperature and concentration are as follows: splay $K_{11} = 4.3$ pN, twist $K_{22} = 0.7$ pN, and bend $K_{33} = 23$ pN (*39*); the rotational viscosity is estimated as $\gamma_1 \sim 20$ kg m^{-1}s^{-1} from the time of director relaxation in a magnetically realigned cell. Subdiffusive behavior is observed again, with $\tau_{sub}^{\|}$= 0.37 s, $\tau_{sub}^{\perp}$= 0.46 s, $\alpha_{\|} = 0.4$ and $\alpha_{\perp} = 0.53$, Fig. S12. At longer times, diffusion is normal, with $D_{\|} = 6.8\times10^{-17}$ m^{2}s^{-1} and $D_{\perp} = 4.5\times10^{-17}$ m^{2}s^{-1}. In the isotropic phase, Fig. S12A, diffusion is normal and isotropic $D_{iso} = 3.2\times10^{-14}$ m^{2}s^{-1}.

4. Scaling exponents and MSD in log-log coordinates

The exponents in the power laws presented in the main text for 5 μm silica particle in IS-8200 were obtained from fitting the data by a single power law in each othe domains, namely, normal domain ($\tau > \tau_{\text{sub}}$), Fig. S13A, subdiffusive domain ($\tau_{\text{sup}} < \tau < \tau_{\text{sub}}$), Fig.S13B, and superdiffusive domain ($\tau < \tau_{\text{sup}}$, down to 0.1 s), Fig.S13C. To help in visualization of data in terms of power laws, we present the log-log plots of MSD vs time lag for 5 μm silica particles diffusing in the nematic phases of IS-8200 (Fig.S13D), 5CB (Fig.S14), and chromonic DSCG (Fig.S15). Although the plots in Figs. S13-S15 do show the deviations from the classic normal diffusion regimes when the time lags become shorter, they do not offer a straightforward protocol to extract the values of α's and τ's (*27*).

Supporting Figures

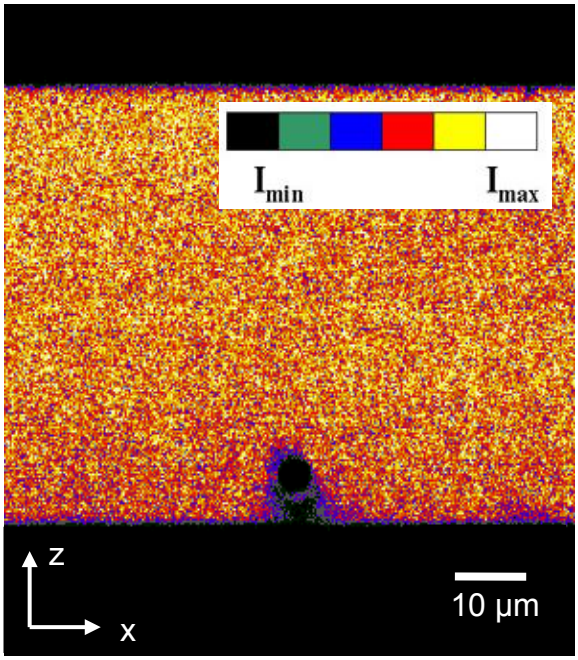

Fig. S1. Levitation of a sphere in nematic LC IS-8200. Fluorescent confocal polarizing microscopy texture of a vertical cross-section of a nematic cell of thickness 50 μm filled with IS-8200 and a small amount (< 0.01wt%) of fluorescent dye *n, n'-bis* (2,5-di-tert-butylphenyl)-3,4,9,10-perylen-edicarboximide (BTBP). The glass sphere of diameter 5 μm levitates at the height about 5 μm from the bottom plate. The shadow below the sphere results from light scattering.

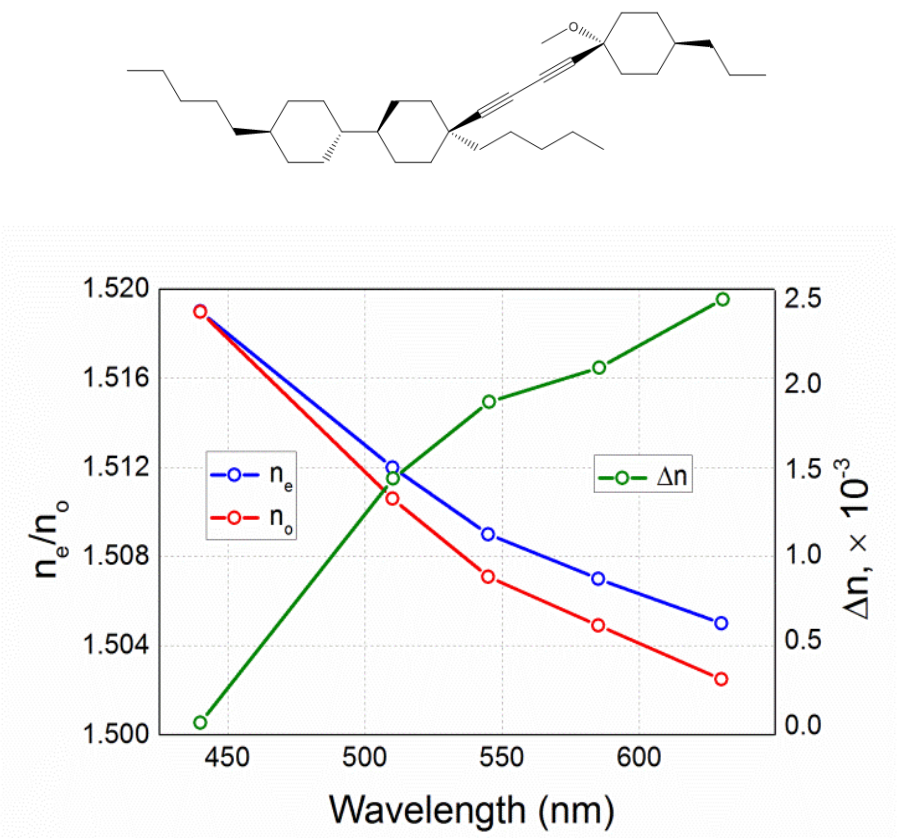

Fig. S2. Nematic liquid crystal IS-8200. (**A**) Chemical structure; (**B**) wavelength dependence of the refractive indices and birefringence Δn.

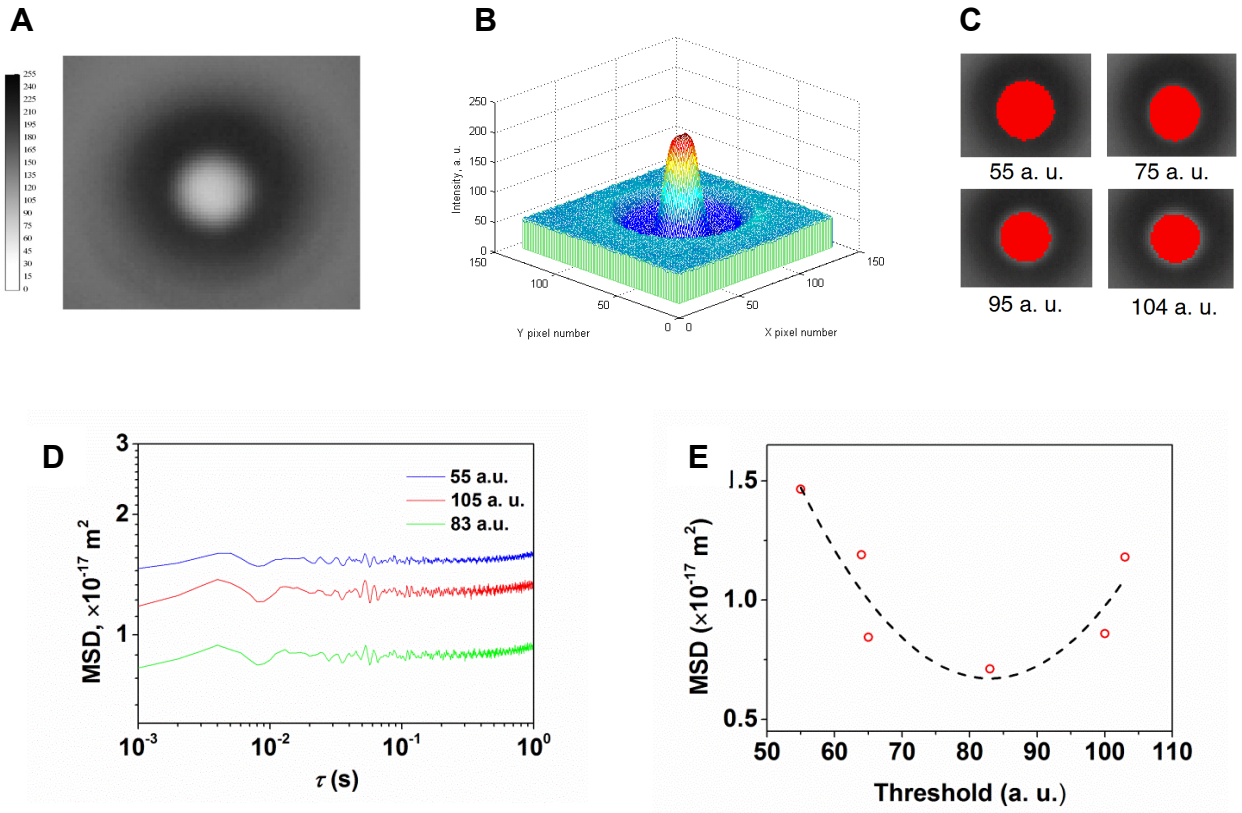

Fig. S3. Determination of particle's position. (**A**) Grayscale image of 5 μm particle glued to the bottom substrate of the cell. (**B**) Intensity profile of the particle image. (**C**) Images of the particle recorded at different intensity threshold levels. Red area consists of pixels that are used to calculate the particle's center coordinates. (**D**) MSD of a glued particle at different levels of threshold intensity. (**E**) The optimum value of intensity threshold is determined from the minimum of MSD for the glued particle.

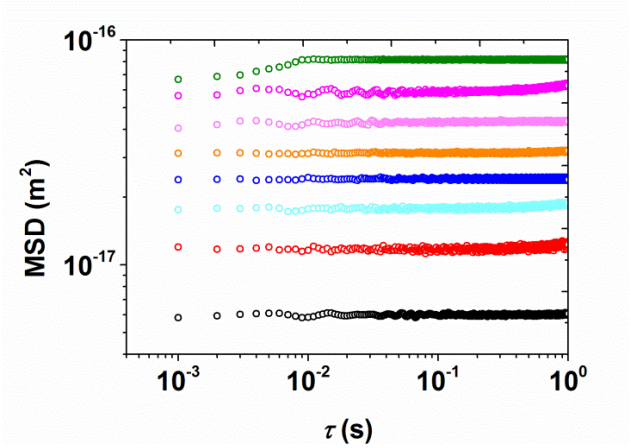

Substance	$\sqrt{\langle \Delta x^2 \rangle}$, nm
5CB	10
IS-8200	7
IS-8200 isotropic	6.6
5CB isotropic	5.7
DSCG	5
Glycerol	4.3
Water	3.5
Dry particle	2.5

Fig. S4. Apparent displacement of particle. Apparent MSD versus time lag for immobilized silica spheres of diameter 5 μm in five different cells (all of thickness 50 μm) filled with three types of a liquid crystals, water, glycerol. Data for an empty cell are labelled as "dry particle". Normal surface anchoring. Higher birefringence results in a higher apparent displacements.

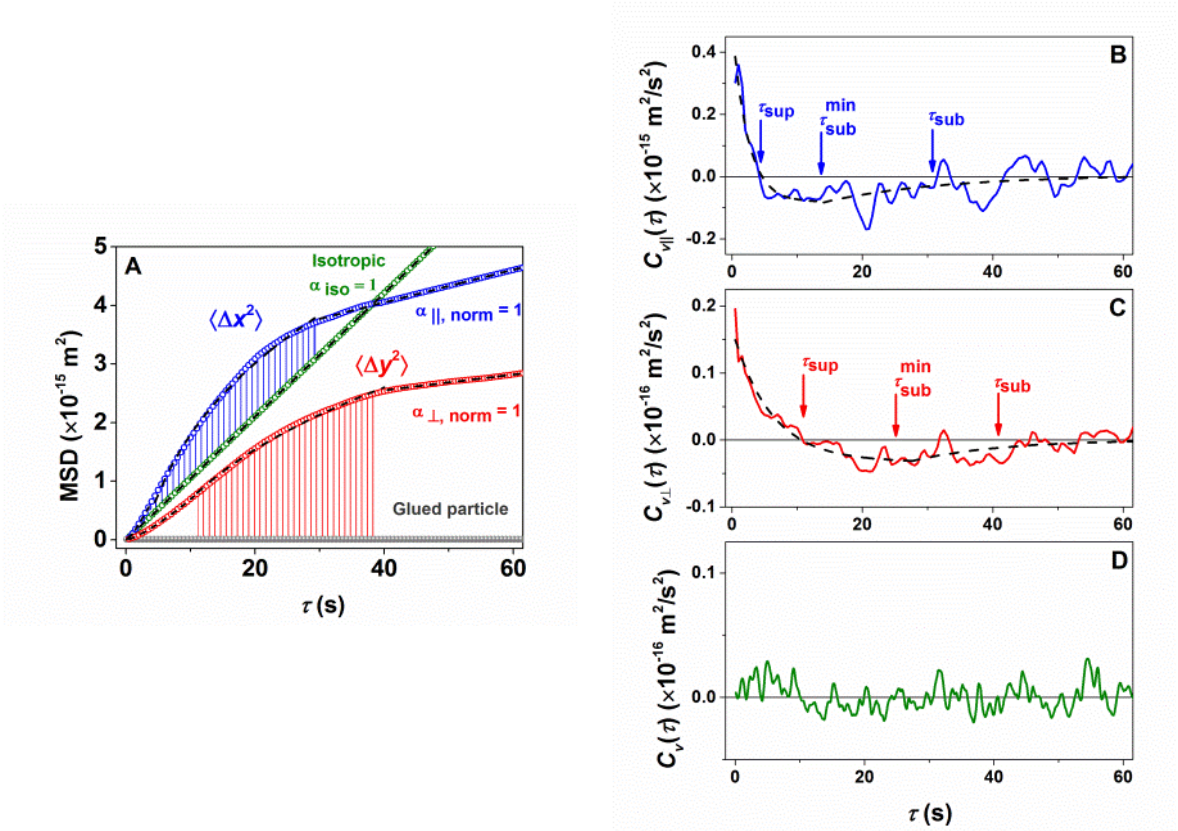

Fig. S5. MSDs and velocity autocorrelation functions of 5 µm silica spheres with tangential surface anchoring in IS-8200. (A) MSD versus time lag for tangentially anchored sphere in the isotropic ($T = 60°C$) and nematic ($T = 50°C$) phases of IS-8200, in the direction parallel (x) and perpendicular (y) to the overall director $\hat{\mathbf{n}}_0$. The bottom curve represents apparent MSD of a particle glued to the cell substrate. Cell thickness 50 µm. **(B)** Velocity autocorrelation function for the tangentially anchored sphere moving parallel to $\hat{\mathbf{n}}_0$ and **(C)** perpendicular to $\hat{\mathbf{n}}_0$. **(D)** The same for the isotropic phase. Dashed lines in **(A)** are least-square fits.

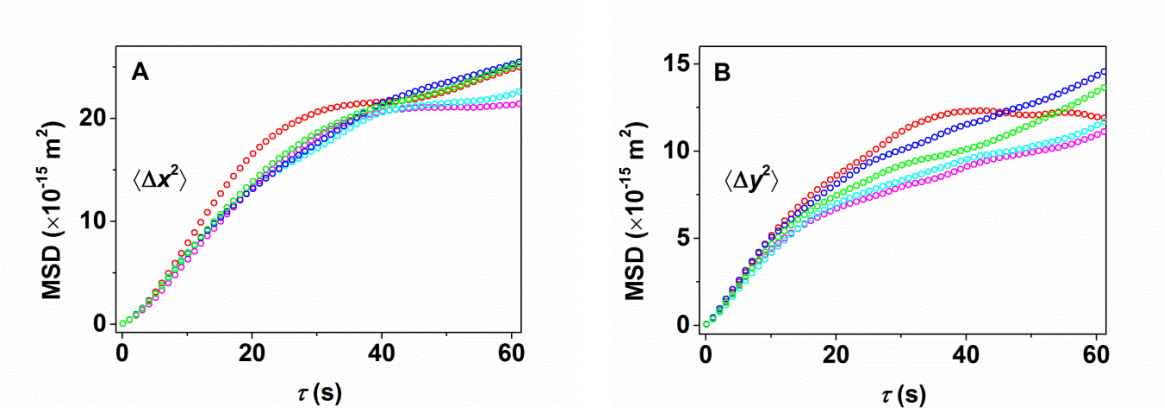

Fig. S6. MSD vs time lag dependencies for different samples. MSD versus time lag for five silica spheres of diameter 5 μm in five different cells (all of thickness 50 μm). Normal surface anchoring. The particles are diffusing in the nematic ($T = 50°C$) phase of IS-8200. The MSD is measured in the directions parallel (**A**) and perpendicular (**B**) to the director.

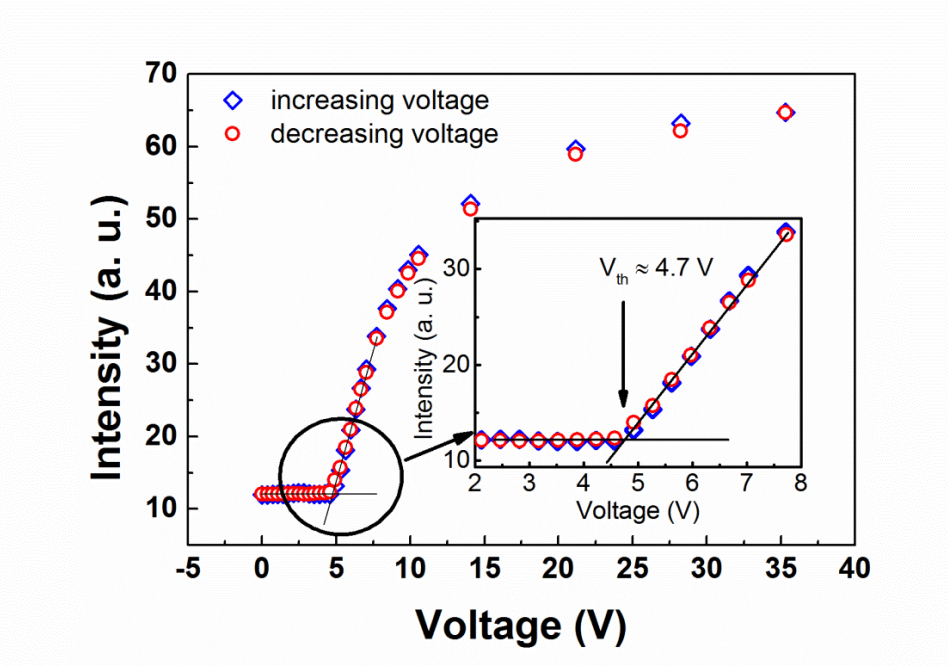

Fig. S7. Electric field induced Frederiks bend transition in IS-8200. Intensity of transmitted light as a function of applied voltage. Cell with homeotropic alignment, crossed polarizers. Cell thickness 20 μm.

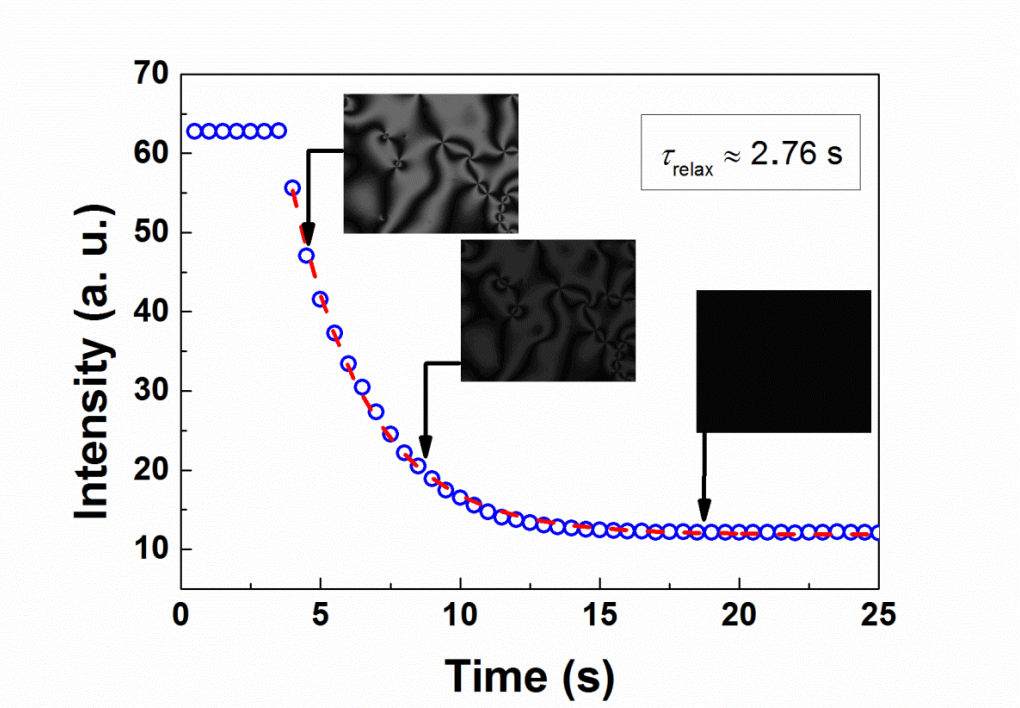

Fig. S8. Relaxation time of bend deformation in IS-8200. Intensity of transmitted light as a function of time after voltage is switched off. Homeotropic cell of thickness 20 μm, crossed polarizers.

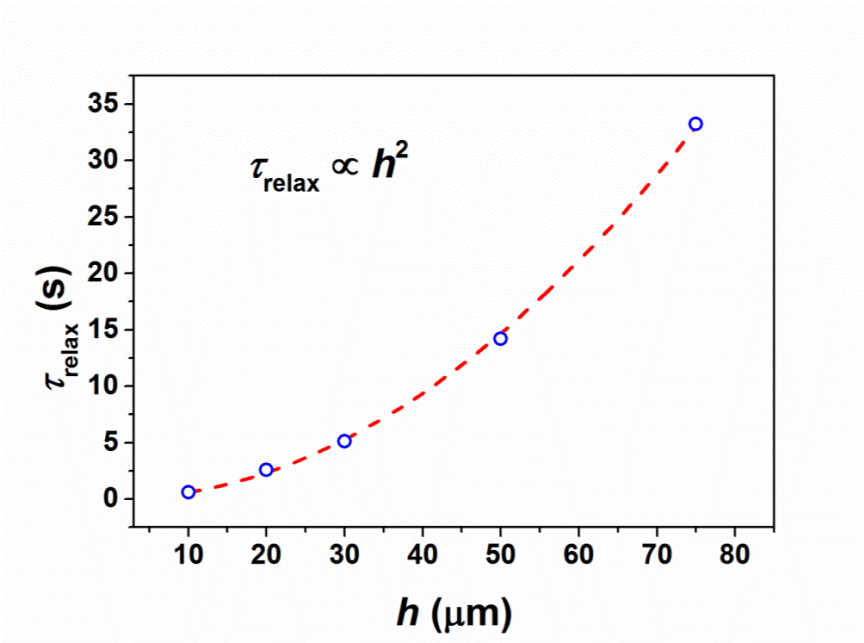

Fig. S9. Scaling of relaxation time of bend deformation. Relaxation time versus cell thickness. IS-8200 in a homeotropic cell.

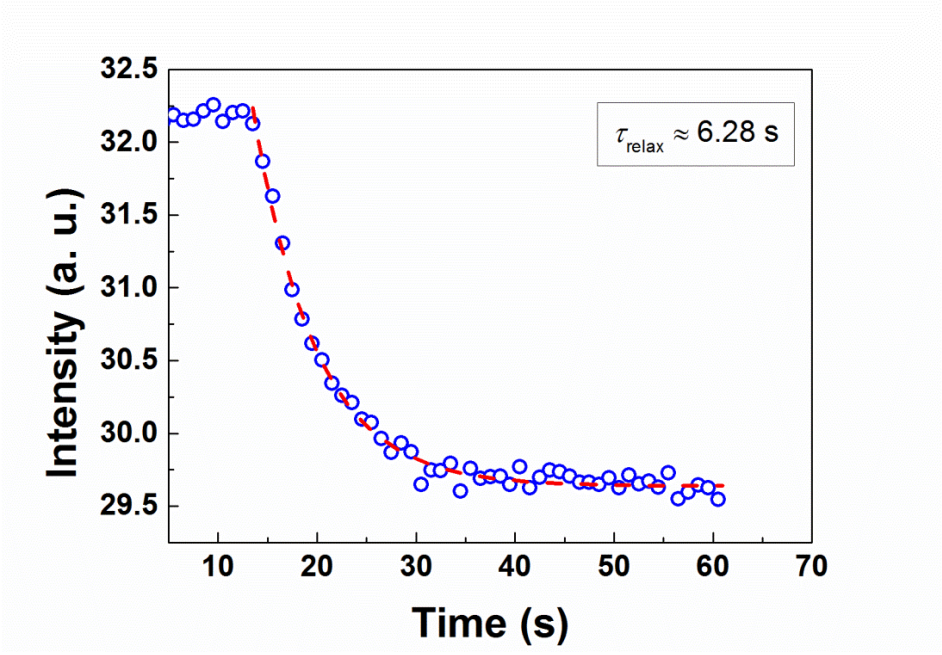

Fig. S10. Relaxation time of twist deformation in IS-8200. Dynamics of light transmittance for a relaxation of twist deformation. IS-8200 in a planar cell of thickness 50 μm. Crossed polarizers.

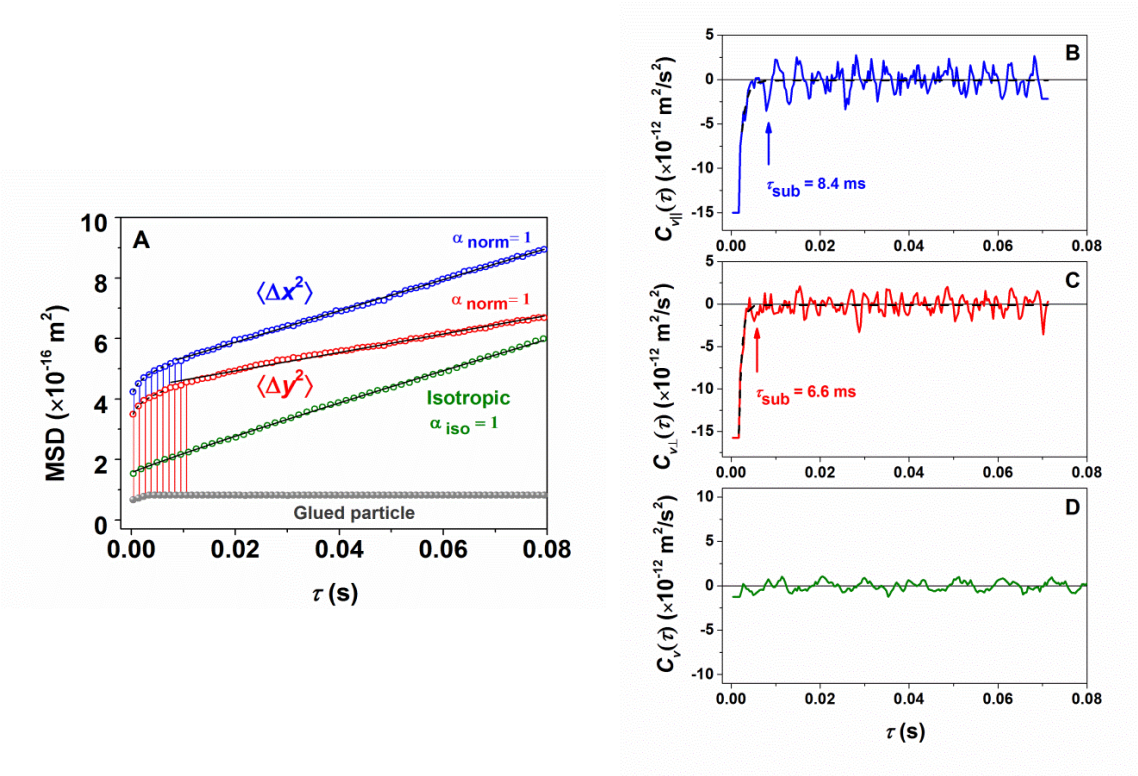

Fig. S11. MSDs and velocity autocorrelation functions of normally anchored silica sphere of diameter 5 μm diffusing in 5CB. (**A**) MSD vs time lag for colloidal particles (diameter 5 μm) diffusing in 5CB, in the directions parallel (x) and perpendicular (y) to the director. The bottom curve represents apparent MSD of immobilized particles in nematic phase. Cell thickness 50 μm. (**B**) Correlation function for the normally anchored sphere moving in the nematic parallel and (**C**) perpendicular to the director. (**D**) Correlation function for the isotropic phase of 5CB.

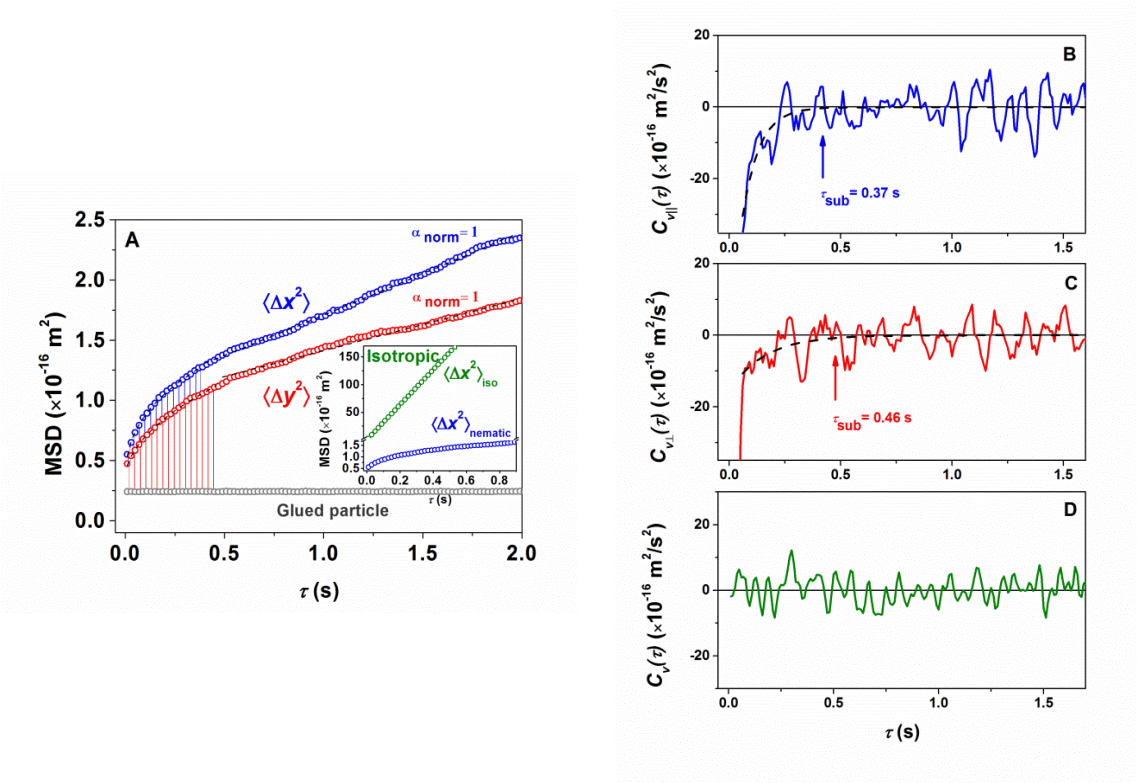

Fig. S12. MSDs and velocity autocorrelation functions of tangentially anchored silica spheres diffusing in DSCG. (**A**) MSD vs time lag for colloidal particles (diameter $5\ \mu m$) diffusing in DSCG, in the directions parallel (x) and perpendicular (y) to the overall director. The bottom curve represents apparent MSD of immobilized particles in the nematic phase. Cell thickness 50 μm. Inset: $\langle \Delta x^2(\tau) \rangle$ for nematic ($22^\circ C$) and isotropic ($40^\circ C$) phase. (**B**) Correlation function for the normally anchored sphere moving in the nematic parallel to the overal director and (**C**) perpendicular to it. (**D**) Correlation function for the isotropic phase of DSCG.

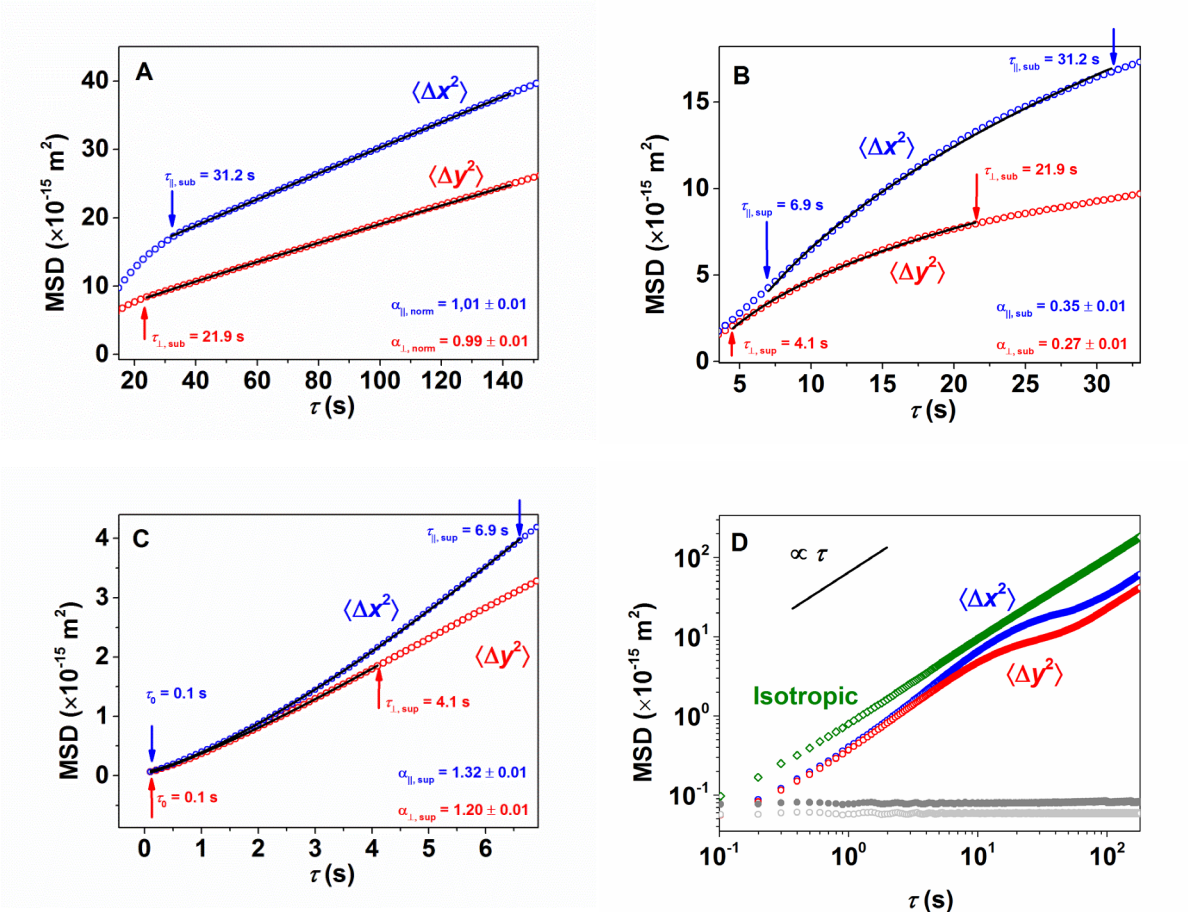

Fig. S13. MSD vs time lag for 5 µm silica sphere (normal anchoring) diffusing in IS-8200. (**A**) normal regime, (B) subdiffusive regime; (C) superdiffusive regime; (**D**) the same data for all three regimes plotted as a single MSD vs. time lag dependence in log-log coordinates. Solid lines in (**A-C**) are power law fits. The two bottom curves in (**D**) represent apparent MSDs of an immobilized particle in the isotropic (open circles) and nematic (filled circles) phases.

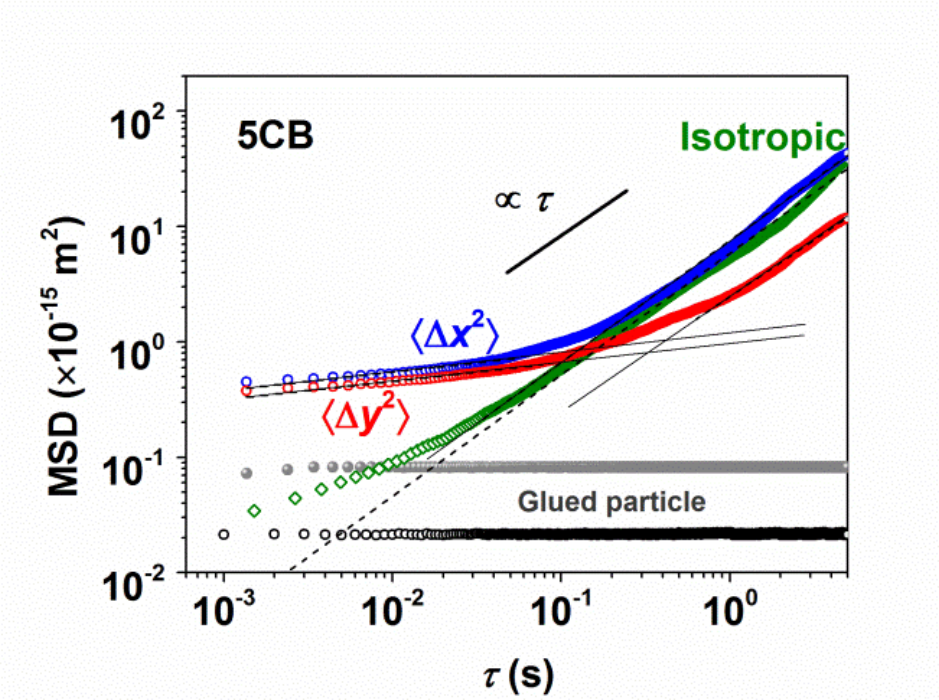

Fig. S14. MSD vs time lag for 5 µm silica sphere (normal anchoring) diffusing in 5CB plotted in log-log coordinates. The two bottom curves represent apparent MSDs of an immobilazed particle in the isotropic (open circles) and nematic (grey filled circles) phases.

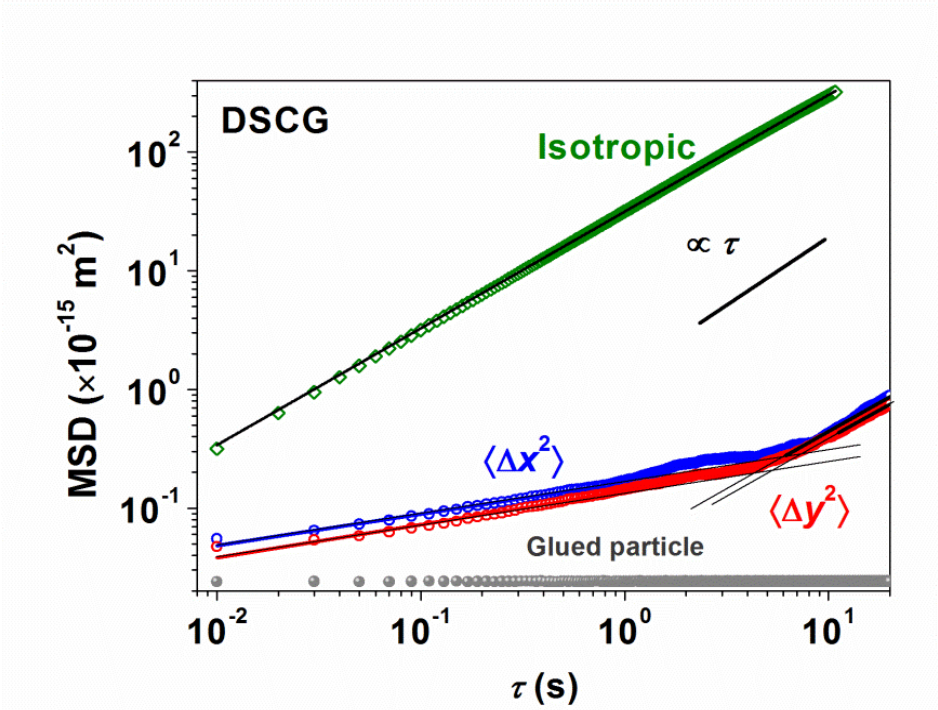

Fig. S15. MSD vs time lag for 5 µm silica sphere diffusing in lyotropic chromonic liquid crystal DSCG.

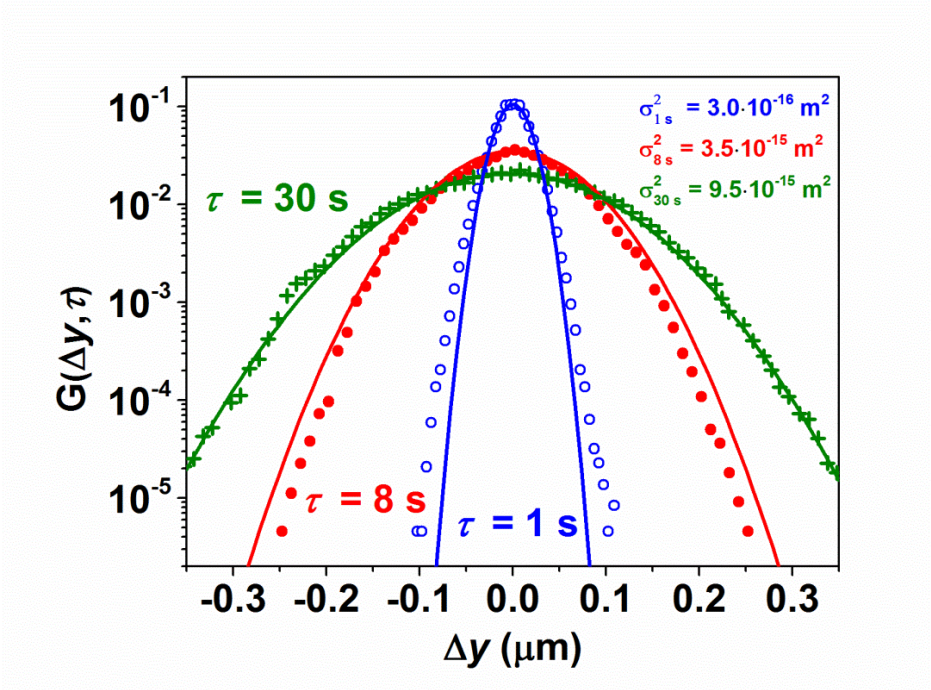

Fig. S16. Probability distribution of particle displacement perpendicular to the director $\hat{\mathbf{n}}_0$, for different time lags, 1 s, 8 s, 30 s. 5 μm silica sphere in IS-8200, perpendicular anchoring, $T = 50°C$. The solid lines are Gaussian fits. The data obtained from a sample of 200,000 single particle's trajectory steps.

Supporting table

Table S1. Physical properties of nematic liquid crystal IS-8200

Birefringence, Δn $(\lambda = 510$ nm$)$	0.0015
Dielectric anisotropy, $\Delta\varepsilon$	-1.5
Rotational viscosity, γ_1	2478 mPa
Phase diagram	$\mathrm{Cr} \xrightarrow{47.0°\mathrm{C}} \mathrm{N} \xrightarrow{52.3°\mathrm{C}} \mathrm{I}$

Table S2. Characteristic times and $\alpha_{\parallel,\perp}$ for different diffusion regimes for d = 5 μm silica spheres of the different anchoring conditions dispersed in IS-8200

Type of director orientation around the sphere	Superdiffusion		Subdiffusion	
	$\parallel$	$\perp$	$\parallel$	$\perp$
Dipolar structure, normal anchoring	$\alpha_{\parallel} = 1.2$ $\tau_{sup}^{\parallel}$ =6.9 s	$\alpha_{\perp} = 1.3$ $\tau_{sup}^{\perp}$ =4.2 s	$\alpha_{\parallel} = 0.4$ $\tau_{sub}^{\parallel}$ =31.2 s $\tau_{sub}^{min,\parallel}$ =14.1 s	$\alpha_{\perp} = 0.3$ $\tau_{sub}^{\perp}$ =21.9 s $\tau_{sub}^{min,\perp}$ =9.7 s
Quadrupolar structure, tangential anchoring	$\alpha_{\parallel} = 1.2$ $\tau_{sup}^{\parallel}$ =4.1 s	$\alpha_{\perp} = 1.3$ $\tau_{sup}^{\perp}$ =10.2 s	$\alpha_{\parallel} = 0.3$ $\tau_{sub}^{\parallel}$ =29.3 s $\tau_{sub}^{min,\parallel}$ =13.7 s	$\alpha_{\perp} = 0.3$ $\tau_{sub}^{\perp}$ =42.7 s $\tau_{sub}^{min,\perp}$ =25.2 s

References

1. W. T. Coffey, Y. P. Kalmykov, J. T. Waldron, *The Langevin Equation: With Applications in Physics, Chemistry and Electrical Engineering* (World Scientific, Singapore, 1996).

2. A. Einstein, *Ann. Phys.* **17**, 549 (1905).

3. J. Sprakel, J. van der Gucht, M. A. Cohen Stuart, N. A. M. Besseling, Brownian particles in transient polymer networks. *Phys. Rev. E* **77**, 061502 (2008). doi:10.1103/PhysRevE.77.061502 Medline

4. I. Y. Wong, M. L. Gardel, D. R. Reichman, E. R. Weeks, M. T. Valentine, A. R. Bausch, D. A. Weitz, Anomalous diffusion probes microstructure dynamics of entangled F-actin networks. *Phys. Rev. Lett.* **92**, 178101 (2004). doi:10.1103/PhysRevLett.92.178101 Medline

5. M. M. Alam, R. Mezzenga, Particle tracking microrheology of lyotropic liquid crystals. *Langmuir* **27**, 6171–6178 (2011). doi:10.1021/la200116e Medline

6. X. L. Wu, A. Libchaber, Wu and Libchaber reply on dispersion of passive particles in a concentrated suspension of swimming bacteria. *Phys. Rev. Lett.* **86**, 557 (2001). doi:10.1103/PhysRevLett.86.557 Medline

7. A. Ott, J. P. Bouchaud, D. Langevin, W. Urbach, Anomalous diffusion in “living polymers”: A genuine Levy flight? *Phys. Rev. Lett.* **65**, 2201–2204 (1990). doi:10.1103/PhysRevLett.65.2201 Medline

8. Y. Gambin, G. Massiera, L. Ramos, C. Ligoure, W. Urbach, Bounded step superdiffusion in an oriented hexagonal phase. *Phys. Rev. Lett.* **94**, 110602 (2005). doi:10.1103/PhysRevLett.94.110602 Medline

9. R. Ganapathy, A. K. Sood, S. Ramaswamy, Superdiffusion of concentration in wormlike-micelle solutions. *Europhys. Lett.* **77**, 18007 (2007). doi:10.1209/0295-5075/77/18007

10. R. Angelico, A. Ceglie, U. Olsson, G. Palazzo, L. Ambrosone, Anomalous surfactant diffusion in a living polymer system. *Phys. Rev. E* **74**, 031403 (2006). doi:10.1103/PhysRevE.74.031403 Medline

11. T. G. Mason, D. A. Weitz, Optical measurements of frequency-dependent linear viscoelastic moduli of complex fluids. *Phys. Rev. Lett.* **74**, 1250–1253 (1995). doi:10.1103/PhysRevLett.74.1250 Medline

12. R. W. Ruhwandl, E. M. Terentjev, Friction drag on a particle moving in a nematic liquid crystal. *Phys. Rev. E* **54**, 5204–5210 (1996). doi:10.1103/PhysRevE.54.5204 Medline

13. H. Stark, D. Ventzki, M. Reichert, Recent developments in the field of colloidal dispersions in nematic liquid crystals: The Stokes drag. *J. Phys. Condens. Matter* **15**, S191–S196 (2003). doi:10.1088/0953-8984/15/1/324

14. J. C. Loudet, P. Hanusse, P. Poulin, Stokes drag on a sphere in a nematic liquid crystal. *Science* **306**, 1525 (2004). doi:10.1126/science.1102864 Medline

15. G. M. Koenig, Jr., R. Ong, A. D. Cortes, J. A. Moreno-Razo, J. J. de Pablo, N. L. Abbott, Single nanoparticle tracking reveals influence of chemical functionality of nanoparticles on local ordering of liquid crystals and nanoparticle diffusion coefficients. *Nano Lett.* **9**, 2794–2801 (2009). doi:10.1021/nl901498d Medline

16. M. Škarabot, I. Muševič, Direct observation of interaction of nanoparticles in a nematic liquid crystal. *Soft Matter* **6**, 5476–5481 (2010). doi:10.1039/c0sm00437e

17. J. A. Moreno-Razo, E. J. Sambriski, G. M. Koenig, E. Díaz-Herrera, N. L. Abbott, J. J. de Pablo, Effects of anchoring strength on the diffusivity of nanoparticles in model liquid-crystalline fluids. *Soft Matter* **7**, 6828–6835 (2011). doi:10.1039/c0sm01506g

18. F. Mondiot, J. C. Loudet, O. Mondain-Monval, P. Snabre, A. Vilquin, A. Würger, Stokes-Einstein diffusion of colloids in nematics. *Phys. Rev. E* **86**, 010401 (2012). doi:10.1103/PhysRevE.86.010401 Medline

19. D. Abras, G. Pranami, N. L. Abbott, The mobilities of micro- and nano-particles at interfaces of nematic liquid crystals. *Soft Matter* **8**, 2026–2035 (2012). doi:10.1039/c1sm06794j

20. M. Pumpa, F. Cichos, Slow single-molecule diffusion in liquid crystals. *J. Phys. Chem. B* **116**, 14487–14493 (2012). doi:10.1021/jp307403w Medline

21. See supplementary materials on *Science* Online.

22. P. Poulin, H. Stark, T. C. Lubensky, D. A. Weitz, Novel colloidal interactions in anisotropic fluids. *Science* **275**, 1770–1773 (1997). doi:10.1126/science.275.5307.1770 Medline

23. O. P. Pishnyak, S. Tang, J. R. Kelly, S. V. Shiyanovskii, O. D. Lavrentovich, Levitation, lift, and bidirectional motion of colloidal particles in an electrically driven nematic liquid crystal. *Phys. Rev. Lett.* **99**, 127802 (2007). doi:10.1103/PhysRevLett.99.127802 Medline

24. V. Reiffenrath, M. Bremer, *Anisotropic Organic Materials* (American Chemical Society, Washington, DC, 2001), pp. 195–205.

25. V. M. Kenkre, R. Kühne, P. Reineker, *Z. Phys. B* **41**, 177–180 (1981).

26. H. Scher, M. Lax, Stochastic transport in a disordered solid. I. Theory. *Phys. Rev. B* **7**, 4491–4502 (1973). doi:10.1103/PhysRevB.7.4491

27. N. Kumar, U. Harbola, K. Lindenberg, Memory-induced anomalous dynamics: Emergence of diffusion, subdiffusion, and superdiffusion from a single random walk model. *Phys. Rev. E* **82**, 021101 (2010). doi:10.1103/PhysRevE.82.021101 Medline

28. P. G. de Gennes, J. Prost, *The Physics of Liquid Crystals* (Clarendon, Oxford, 1993).

29. T. C. Lubensky, D. Pettey, N. Currier, H. Stark, Topological defects and interactions in nematic emulsions. *Phys. Rev. E* **57**, 610–625 (1998). doi:10.1103/PhysRevE.57.610

30. D. Voloshchenko, O. P. Pishnyak, S. V. Shiyanovskii, O. D. Lavrentovich, Effect of director distortions on morphologies of phase separation in liquid crystals. *Phys. Rev. E* **65**, 060701 (2002). doi:10.1103/PhysRevE.65.060701 Medline

31. D. S. Martin, M. B. Forstner, J. A. Käs, Apparent subdiffusion inherent to single particle tracking. *Biophys. J.* **83**, 2109–2117 (2002). doi:10.1016/S0006-3495(02)73971-4 Medline

32. I. Muševič, M. Škarabot, U. Tkalec, M. Ravnik, S. Žumer, Two-dimensional nematic colloidal crystals self-assembled by topological defects. *Science* **313**, 954–958 (2006). doi:10.1126/science.1129660 Medline

33. J. C. Crocker, D. G. Grier, Methods of digital video microscopy for colloidal studies. *J. Colloid Interface Sci.* **179**, 298–310 (1996). doi:10.1006/jcis.1996.0217

34. A. Kasper, E. Bartsch, H. Sillescu, Self-diffusion in concentrated colloid suspensions studied by digital video microscopy of core-shell tracer particles. *Langmuir* **14**, 5004–5010 (1998). doi:10.1021/la971089y

35. M. Cui, J. R. Kelly, Temperature dependence of visco-elastic properties of 5CB. *Mol. Cryst. Liq. Cryst.* **331**, 49–57 (1999). doi:10.1080/10587259908047499

36. H. Stark, D. Ventzki, Stokes drag of spherical particles in a nematic environment at low Ericksen numbers. *Phys. Rev. E* **64**, 031711 (2001). doi:10.1103/PhysRevE.64.031711 Medline

37. J. Lydon, Chromonic liquid crystalline phases. *Liq. Cryst.* **38**, 1663–1681 (2011). doi:10.1080/02678292.2011.614720

38. Y. A. Nastishin, H. Liu, T. Schneider, V. Nazarenko, R. Vasyuta, S. V. Shiyanovskii, O. D. Lavrentovich, Optical characterization of the nematic lyotropic chromonic liquid crystals: Light absorption, birefringence, and scalar order parameter. *Phys. Rev. E* **72**, 041711 (2005). doi:10.1103/PhysRevE.72.041711 Medline

39. S. Zhou, Y. A. Nastishin, M. M. Omelchenko, L. Tortora, V. G. Nazarenko, O. P. Boiko, T. Ostapenko, T. Hu, C. C. Almasan, S. N. Sprunt, J. T. Gleeson, O. D. Lavrentovich, Elasticity of lyotropic chromonic liquid crystals probed by director reorientation in a magnetic field. *Phys. Rev. Lett.* **109**, 037801 (2012). doi:10.1103/PhysRevLett.109.037801 Medline